BULLETIN OF THE POLISH ACADEMY OF SCIENCES
TECHNICAL SCIENCES, Vol. 62, No. 3, 2014
DOI: 10.2478/bpasts-2014-0046

A state-space approach for control of NPC type 3-level sine wave inverter used in FOC PMSM drive

T. TARCZEWSKI[1]*, L.M. GRZESIAK[2], A. WAWRZAK[1], K. KARWOWSKI[1], and K. ERWINSKI[1]

[1] Institute of Physics, Faculty of Physics, Astronomy and Informatics, Nicolaus Copernicus University, 5 Grudziadzka St., 87-100 Torun, Poland
[2] Institute of Control and Industrial Electronics, Warsaw University of Technology, 75 Koszykowa St., 00-662 Warsaw, Poland

Abstract. This paper presents the design and analysis process of state feedback controllers for NPC type 3-level sine wave inverter. In order to achieve good dynamic features in a state feedback control an internal model of reference input and a feedforward path are introduced. During synthesis process of the state feedback controllers maximum permissible dynamics of voltage control in the linear range of modulation is taken into account. It is shown that initially gains of the controller and feedforward path are non-stationary and depend on the angular velocity. Stationary approximation of a non-stationary state feedback controller is presented in details. Proposed state feedback control structures for continuous voltage shaping NPC type 3-level voltage source inverter are examined in FOC PMSM drive. The novelty of the presented controller lays in a stationary approximated state feedback control structure designed in terms of maximum permissible dynamics of a voltage control system. Simulation and experimental results (at the level of 3 kW) of the designed control algorithms are included.

Key words: state feedback control, linear-quadratic regulator, 3-level neutral point clamped voltage source inverter, LC filter.

1. Introduction

Based on permanent magnet synchronous motors (PMSM) high performance motion control applications such as metal-working machine tools, robots and satellite trackers require reduction of all sources of pulsating torque such as: non-sinusoidal flux density distribution around the air-gap, variable magnetic reluctance of the air-gap due to stator slots and non-sinusoidal output voltage of the inverter [1–3]. A torque ripple degrades the performance of a drive and produces undesirable mechanical vibration leading to acoustic noise [2]. The methods of reducing torque ripple can be divided into two groups: using complex control techniques, and putting the LC filter between inverter and PMSM. In the first group are: iterative learning control used to reduce periodic torque pulsations [2], adaptive control based on complex model of PMSM [4], control with harmonic cancelation using the pre-programmed current waveforms [5]. In the second group an additional passive filter is required to obtain sinusoidal output voltage waveform of inverter [6]. When typical 2-level inverter is used, an LC filter will be bulky and heavy device. For a specified value of the torque ripple, the weight and overall dimension of LC filter can be reduced if 3-level inverter is used instead of 2-level [7]. Neutral Point Clamped (NPC) 3-level voltage source inverter is a widely used topology of multilevel inverters [8–10].

A sinusoidal output voltage waveform of the 3-level inverter with an output LC filter can be formed in a wide range of the drive operation with the help of the additional voltage control system. Deadbeat controllers [6] or a cascade control structure with classical PI controllers [11] can be applied to shape a sinusoidal output voltage waveform of the inverter. The mathematical model of an inverter with an output LC filter is non-linear and non-stationary [12]. Properties of the model described above cause that, thanks to full vector component decoupling ability, state feedback control is an attractive approach to control the NPC inverter with an output LC filter. Non-stationary gain matrices of the state feedback voltage controller can be obtained using pole placement technique [13] or linear-quadratic optimization method [12]. In both cases coefficients of the designed state feedback controller will be non-stationary (i.e. it depend on the angular velocity). In order to control space vector components of the filter output voltages without steady state error (in a case of step variations of the reference voltages), an internal model of the reference input [14] is added. Further improvement of the dynamic features in state feedback control is possible by introducing a feedforward path into control algorithm [13].

Our primary goal is to design and examine a state-space control system for continuous voltage shaping NPC type 3-level voltage source inverter in terms of minimization PMSM torque ripple caused by a non-sinusoidal output voltage of the inverter. There are two case studies presented here: state feedback with internal model control (SFC1), state feedback with: internal model control, an additional feedforward path and feedback from measurable disturbance (SFC2). During the synthesis process of the state feedback controllers maximum permissible dynamics of voltage control in the linear range of modulation is taken into account. Stationary approximation of a non-stationary state feedback controller is presented in details. Finally, simulation and experimental results of the designed control algorithms are shown.

*e-mail: ttarczewski@fizyka.umk.pl

2. Continuous voltage shaping NPC type 3-level voltage source inverter system

Continuous voltage shaping is realized in a voltage control system which consists of: NPC type 3-level voltage source inverter and output LC filter. The voltage control system described above can be a part of a PMSM drive control system presented in Fig. 1.

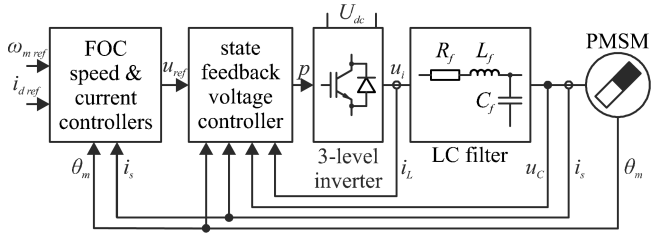

Fig. 1. Schematic diagram of the proposed control system

Three control loops are used to control voltage of the inverter as well as currents and angular velocity of PMSM.

An outer control loops consist of cascade field-oriented control structure with PI type currents and angular velocity controllers [15]. Current control loop is realized in an orthogonal $d-q$ coordinate system that rotates with angular velocity of PMSM.

An inner control loop provides continuous voltage shaping of inverter. Due to non-linear and non-stationary model of inverter with LC filter [12], state feedback control algorithm will be used in a voltage control system. Two different state feedback control structures will be examined in terms of torque ripple reduction.

A mathematical model of the plant (i.e. NPC type 3-level inverter with output LC filter) should be introduced in order to design state feedback controller. Topology of LC filter with voltage and current sensors is presented in Fig. 2.

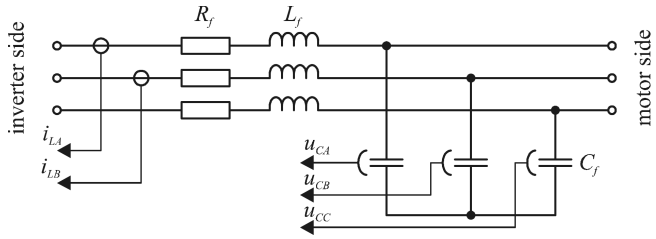

Fig. 2. Topology of LC filter

The model of an output LC filter is written in an orthogonal $d-q$ coordinate system. The expression of voltage and current equation takes the following form [13]:

$$u_{id} = R_f i_{Ld} + L_f \frac{\mathrm{d}i_{Ld}}{\mathrm{d}t} - L_f \omega_k i_{Lq} + u_{Cd}, \tag{1}$$

$$u_{iq} = R_f i_{Lq} + L_f \frac{\mathrm{d}i_{Lq}}{\mathrm{d}t} + L_f \omega_k i_{Ld} + u_{Cq}, \tag{2}$$

$$i_{Cd} = C_f \frac{\mathrm{d}u_{Cd}}{\mathrm{d}t} - C_f \omega_k u_{Cq}, \tag{3}$$

$$i_{Cq} = C_f \frac{\mathrm{d}u_{Cq}}{\mathrm{d}t} + C_f \omega_k u_{Cd}, \tag{4}$$

$$i_{Ld} = i_{Cd} + i_{sd}, \tag{5}$$

$$i_{Lq} = i_{Cq} + i_{sq}, \tag{6}$$

where u_{id}, u_{iq}, i_{Ld}, i_{Lq} are space vector components of filter input voltages and currents, i_{Cd}, i_{Cq} are space vector components of currents in filter capacitance, R_f is filter resistance, L_f is filter inductance, C_f is filter capacitance, ω_k is angular velocity of $d-q$ coordinate system, u_{Cd}, u_{Cq}, i_{sd}, i_{sq} are space vector components of filter output voltages and currents.

In order to design state feedback voltage controller, model of the 3-level NPC type voltage source inverter has to be taken into account. Dynamics of the inverter can be approximated by using proportional element if we assume that: inverter operates in a linear range, dead time of IGBTs are ignored, the switching period is much smaller than the electrical time constant of PMSM. Static model of the 3-level NPC type voltage source inverter can be described as follows [14]:

$$\begin{bmatrix} u_{id} \\ u_{iq} \end{bmatrix} = K_p \begin{bmatrix} u_{pd} \\ u_{pq} \end{bmatrix}, \tag{7}$$

where u_{pd}, u_{pq} are space vector components of inverter control voltages, K_p is gain coefficient of considered inverter. Presented in [14] simulation and experimental results show, that described above static model of the inverter does not introduce any significant error. Proposed model (7) is valid for a typical 2-level inverter as well as for multilevel one.

Now the model of an inverter (7) with an output LC filter (1)–(6) can be rewritten in a standard form of a state equation as follows:

$$\frac{\mathrm{d}x}{\mathrm{d}t} = \boldsymbol{A}(\omega_k)\boldsymbol{x} + \boldsymbol{B}\boldsymbol{u} + \boldsymbol{E}\boldsymbol{d}, \tag{8}$$

where

$$\boldsymbol{x} = \begin{bmatrix} i_{Ld} \\ i_{Lq} \\ u_{Cd} \\ u_{Cq} \end{bmatrix}, \quad \boldsymbol{A}(\omega_k) = \begin{bmatrix} -\frac{R_f}{L_f} & \omega_k & -\frac{1}{L_f} & 0 \\ -\omega_k & -\frac{R_f}{L_f} & 0 & -\frac{1}{L_f} \\ \frac{1}{C_f} & 0 & 0 & \omega_k \\ 0 & \frac{1}{C_f} & -\omega_k & 0 \end{bmatrix},$$

$$\boldsymbol{d} = \begin{bmatrix} i_{sd} \\ i_{sq} \end{bmatrix}, \quad \boldsymbol{B} = \begin{bmatrix} \frac{K_p}{L_f} & 0 \\ 0 & \frac{K_p}{L_f} \\ 0 & 0 \\ 0 & 0 \end{bmatrix},$$

$$\boldsymbol{u} = \begin{bmatrix} u_{pd} \\ u_{pq} \end{bmatrix}, \quad \boldsymbol{E} = \begin{bmatrix} 0 & 0 \\ 0 & 0 \\ -\frac{1}{C_f} & 0 \\ 0 & -\frac{1}{C_f} \end{bmatrix}.$$

Note, that presented above state equation of the inverter with LC filter is non-stationary because the state matrix $\boldsymbol{A}$ depends on angular velocity ω_k.

3. State-space control system design

Our primary goal is to design and examine state-space control system with continuous voltage shaping voltage source inverter in terms of PMSM torque ripple reduction. In order to minimize the weight and overall dimension of LC filter the 3-level NPC type inverter was used. A schematic diagram of the proposed control system is presented in Fig. 3.

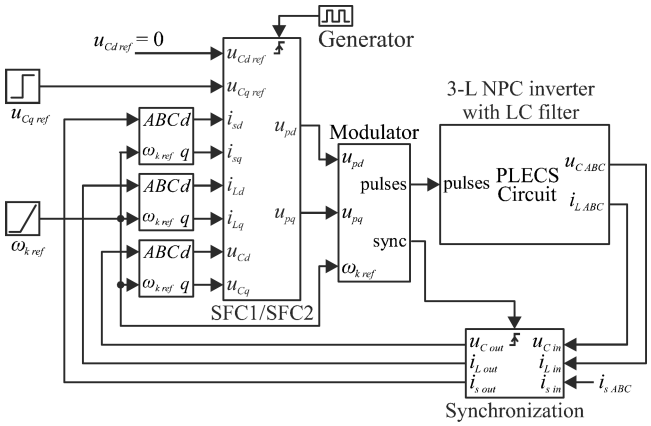

Fig. 3. Block diagram of the voltage control system

The simulation model of the proposed control system was tested in Matlab/Simulink/Plecs. Analyzed discrete state feedback controllers (SFC1 and SFC2) were implemented in triggered subsystem in order to ensure proper generation of discrete control signals. Additional signals of the PMSM phase currents shown in Fig. 3 are required in a state feedback controller with internal model control and with feedforward path (SFC2). Triggered synchronization block was used in order to realize measurements in a midpoint of the PWM pulse length. The sampling interval was set to $T_s = 100\ \mu$s (the switching frequency is equal to $f_s = 10$ kHz).

Block diagram of the control structure with PMSM presented in Fig. 4. was used to examine torque ripple reduction.

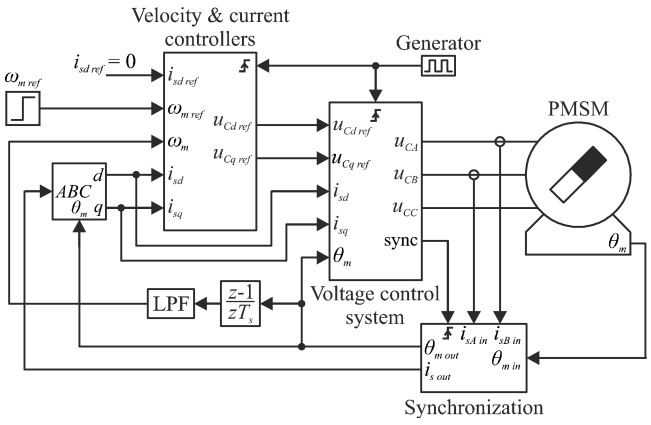

Fig. 4. Block diagram of the PMSM drive

The voltage control system (Fig. 3) described above is a part of a cascade control structure presented in Fig. 4. Discrete PI controllers were used to control angular velocity and space vector components of the PMSM currents. The field-oriented control with zero direct current control strategy was applied [15]. A synthesis procedure of velocity and current controllers was made with an assumption that phase currents should not exceed its nominal value during start-up. The parameter specification of the drive with PMSM and additional moment of inertia J_d are given in Table 1.

Table 1
Drive parameters

Parameter	Value	Unit
P_N	2.76	kW
I_N	5.8	A
T_{eN}	8.8	Nm
Ω_{mN}	314	rad/s
f_s	150	Hz
p	3	
R_s	1.05	Ω
L_s	9.5	mH
K_t	1.64	Nm/A
B_m	1.4×10^{-3}	Nms/rad
J_m	6.2×10^{-4}	kgm^2
J_d	2.45×10^{-2}	kgm^2

Simulation as well as experimental results were confirmed for DC-link voltage $U_{dc} = 120$ V.

3.1. State feedback control structure with internal model control (SFC1).

In order to control space vector components of the filter output voltages without steady-state error (in a case of step variations of the reference voltages), an internal model of the reference input should be added [13, 14].

An augmented state equation, after introduction the internal input model and assumption, that space vector components of filter output currents are omitted, takes the following form:

$$\frac{\mathrm{d}x_i}{\mathrm{d}t} = \boldsymbol{A}_i(\omega_k)\boldsymbol{x}_i + \boldsymbol{B}_i\boldsymbol{u}_i + \boldsymbol{F}_i\boldsymbol{r}_i, \tag{9}$$

where

$$\boldsymbol{x}_i = \begin{bmatrix} i_{Ld} \\ i_{Lq} \\ u_{Cd} \\ e_{Cd} \\ u_{Cq} \\ e_{Cq} \end{bmatrix},$$

$$\boldsymbol{A}_i(\omega_k) = \begin{bmatrix} -\dfrac{R_f}{L_f} & \omega_k & -\dfrac{1}{L_f} & 0 & 0 & 0 \\ -\omega_k & -\dfrac{R_f}{L_f} & 0 & 0 & -\dfrac{1}{L_f} & 0 \\ \dfrac{1}{C_f} & 0 & 0 & 0 & \omega_k & 0 \\ 0 & 0 & 1 & 0 & 0 & 0 \\ 0 & \dfrac{1}{C_f} & -\omega_k & 0 & 0 & 0 \\ 0 & 0 & 0 & 0 & 1 & 0 \end{bmatrix},$$

$$\boldsymbol{B}_i = \begin{bmatrix} \frac{K_p}{L_f} & 0 \\ 0 & \frac{K_p}{L_f} \\ 0 & 0 \\ 0 & 0 \\ 0 & 0 \\ 0 & 0 \end{bmatrix}, \qquad \boldsymbol{u}_i = \boldsymbol{u},$$

$$\boldsymbol{F}_i = \begin{bmatrix} 0 & 0 \\ 0 & 0 \\ 0 & 0 \\ 0 & 0 \\ -1 & 0 \\ 0 & -1 \end{bmatrix}, \qquad \boldsymbol{r}_i = \begin{bmatrix} u_{Cd\,ref} \\ u_{Cq\,ref} \end{bmatrix}.$$

Introduced in an augmented state Eq. (9) new state variables e_{Cd} and e_{Cq} correspond to the integral of the output voltages error as follows:

$$\boldsymbol{e}_C(t) = \int_0^t [\boldsymbol{u}_C(\tau) - \boldsymbol{u}_{C\,ref}(\tau)]\,\mathrm{d}\tau, \tag{10}$$

where

$$\boldsymbol{e}_C = \begin{bmatrix} e_{Cd} \\ e_{Cq} \end{bmatrix}, \qquad \boldsymbol{u}_C = \begin{bmatrix} u_{Cd} \\ u_{Cq} \end{bmatrix}, \qquad \boldsymbol{u}_{C\,ref} = \begin{bmatrix} u_{Cd\,ref} \\ u_{Cq\,ref} \end{bmatrix}, \tag{11}$$

u_{Cdref} and u_{Cqref} are reference values of the voltage space vector components.

The control law for a non-stationary system described by state Eq. (9) can be calculated from the following formula:

$$u = -K(\omega_k)\boldsymbol{x}_i = -\boldsymbol{K}_x(\omega_k)\boldsymbol{x} - \boldsymbol{K}_{ec}(\omega_k)\boldsymbol{e}_C, \tag{12}$$

where $\boldsymbol{K}(\omega_k)$, $\boldsymbol{K}_x(\omega_k)$, $\boldsymbol{K}_{ec}(\omega_k)$ are non-stationary gain matrices of the state feedback controller SFC1.

In order to design discrete state feedback controller suitable to implement in a DSP system, the control law (12) must be rewritten in a discrete form [16]:

$$\begin{aligned} u(n) &= -K(\omega_k)\boldsymbol{x}_i(n) \\ &= -\boldsymbol{K}_x(\omega_k)\boldsymbol{x}(n) - \boldsymbol{K}_{ec}(\omega_k)\boldsymbol{e}_C(n), \end{aligned} \tag{13}$$

where n is discrete sample time index. Depicted in (13) discrete form of the error vector $\boldsymbol{e}_c$ was obtained by using the backward Euler integration algorithm:

$$\boldsymbol{e}_C(n) = \boldsymbol{e}_C(n-1) + T_s[\boldsymbol{u}_C(n) - \boldsymbol{u}_{C\,ref}(n)], \tag{14}$$

where T_s is the sampling interval.

The discrete linear-quadratic optimization method [17] was used to obtain gain coefficients of SFC1 controller at the operating points defined by the actual value of the angular velocity $\omega_k \in [-942;\ 942]$ rad/s. Matlab's *lqrd* command has been used to calculate appropriate matrices.

In order to calculate non-stationary gain values of the SFC1 controller the following penalty matrices has been chosen:

$$\begin{aligned} \boldsymbol{R} &= diag([r_1\ r_2]), \\ \boldsymbol{Q} &= diag([q_1\ q_2\ q_3\ q_4\ q_5\ q_6]), \end{aligned} \tag{15}$$

where $q_1 = q_2 = q_3 = q_5 = 1 \times 10^{-2}$, $q_4 = q_6 = 5 \times 10^6$, $r_1 = r_2 = 6 \times 10^2$.

Values of the gain matrices (15) were determined by a trial-and-error procedure in order to: provide zero steady state error of u_{Cd} and u_{Cq} for step changes of u_{Cdref} and u_{Cqref}, achieve maximum permissible dynamics of voltage control in the linear range of modulation.

After computation of the SFC1 gain coefficients:

$$\begin{aligned} \boldsymbol{K}_x(\omega_k) &= \begin{bmatrix} k_{d1}(\omega_k) & k_{d2}(\omega_k) & k_{d3}(\omega_k) & k_{d4}(\omega_k) \\ k_{q1}(\omega_k) & k_{q2}(\omega_k) & k_{q3}(\omega_k) & k_{q4}(\omega_k) \end{bmatrix}, \\ \boldsymbol{K}_{ec}(\omega_k) &= \begin{bmatrix} k_{d5}(\omega_k) & k_{d6}(\omega_k) \\ k_{q5}(\omega_k) & k_{q6}(\omega_k) \end{bmatrix} \end{aligned} \tag{16}$$

a polynomial approximation was used to determine the mathematical functions that approximate dependencies between the controller's gains and the angular velocity. With the help of Matlab's *polyfit* and *polyval* commands it was found that coefficients: $k_{d1}(\omega_k)$, $k_{d3}(\omega_k)$, $k_{d5}(\omega_k)$, $k_{q2}(\omega_k)$, $k_{q4}(\omega_k)$, $k_{q6}(\omega_k)$ are quadratic functions of the angular velocity. Dependencies between coefficients: $k_{d2}(\omega_k)$, $k_{d4}(\omega_k)$, $k_{d6}(\omega_k)$, $k_{q1}(\omega_k)$, $k_{q3}(\omega_k)$, $k_{q5}(\omega_k)$ and the angular velocity can be approximated by linear functions respectively.

Based on simulation as well as experimental test results of the described in a previous section control system it was found that all coefficients (16) of the SFC1 can be adequately approximated by constant values (independent of the angular velocity). Constant coefficients of the SFC1 were expressed as mean values of non-stationary coefficients presented above. It should be noted that all linear functions are symmetric about the origin (mean values of $k_{d2}(\omega_k)$, $k_{d4}(\omega k)$, $k_{d6}(\omega_k)$, $k_{q1}(\omega_k)$, $k_{q3}(\omega_k)$, $k_{q5}(\omega_k)$ are equal to zero).

Finally, constant gain coefficients of SFC1 calculated for system (9) with parameters given in table 2 and for penalty matrices (15) are as follows:

$$\begin{aligned} \boldsymbol{K}_x &= \begin{bmatrix} 0.17 & 0 & 0.024 & 0 \\ 0 & 0.17 & 0 & 0.024 \end{bmatrix}, \\ \boldsymbol{K}_{ec} &= \begin{bmatrix} 67.87 & 0 \\ 0 & 67.87 \end{bmatrix}. \end{aligned} \tag{17}$$

Table 2
Voltage source inverter and LC filter parameters

Parameter	Value	Unit
R_f	100	mΩ
L_f	2.1	mH
C_f	58	μF
K_p	60	

Note that the highest values of SFC1 coefficients (17) are related to state variables e_{Cd} and e_{Cq}.

The final version of the designed state feedback controller SFC1 is shown in Fig. 5.

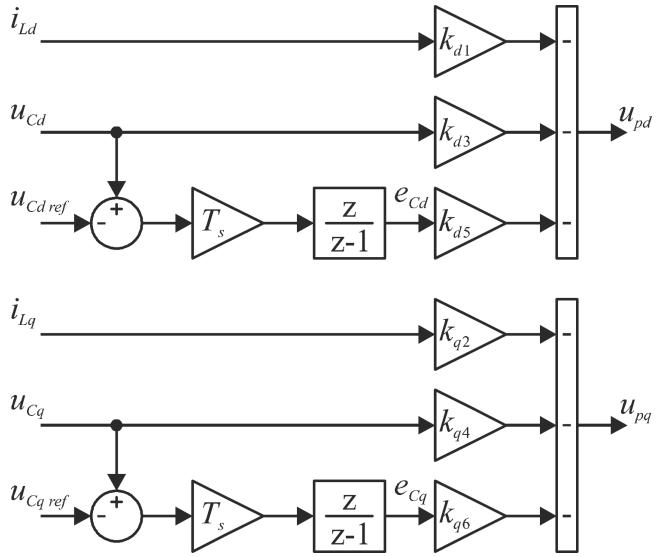

Fig. 5. Block diagram of the designed state feedback controller (SFC1)

At first, the accuracy of the voltage shaping have been investigated and results for SFC1 are shown in Fig. 6.

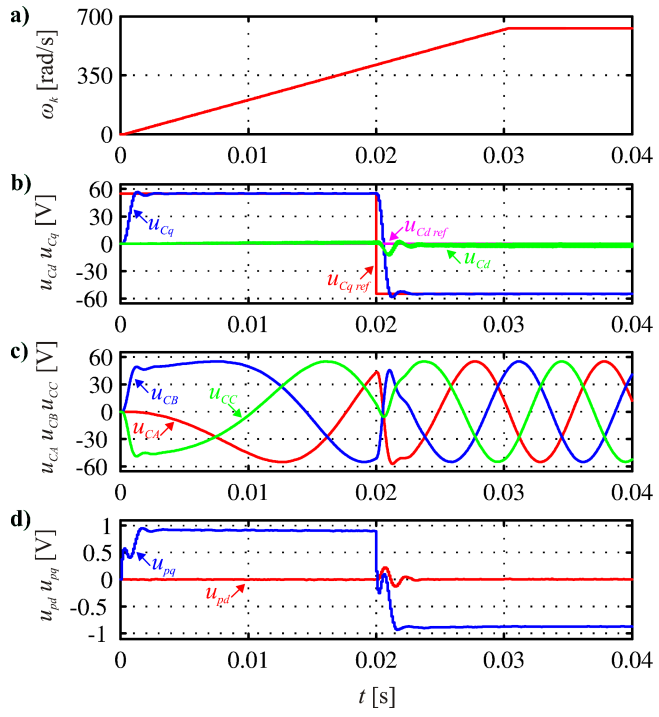

Fig. 6. Response of voltage control loop with SFC1 to step change of reference voltage $u_{Cq\,ref}$ and linear change of angular velocity ω_k

It can be seen from Fig. 6b that space vector components of the filter output voltages are controlled properly. The 5% settling time of u_{Cq} is about 1 ms. Dynamic properties of the voltage control loop are limited by the maximum permissible value of the control signal (i.e. $|u_{pd}| \leq 1$ and $|u_{pq}| \leq 1$). Note that phase voltages presented in Fig. 6c are sinusoidal in a steady-state.

The operation of PMSM drive fed from voltage control system (Fig. 3) with SFC1 has been illustrated in Fig. 7.

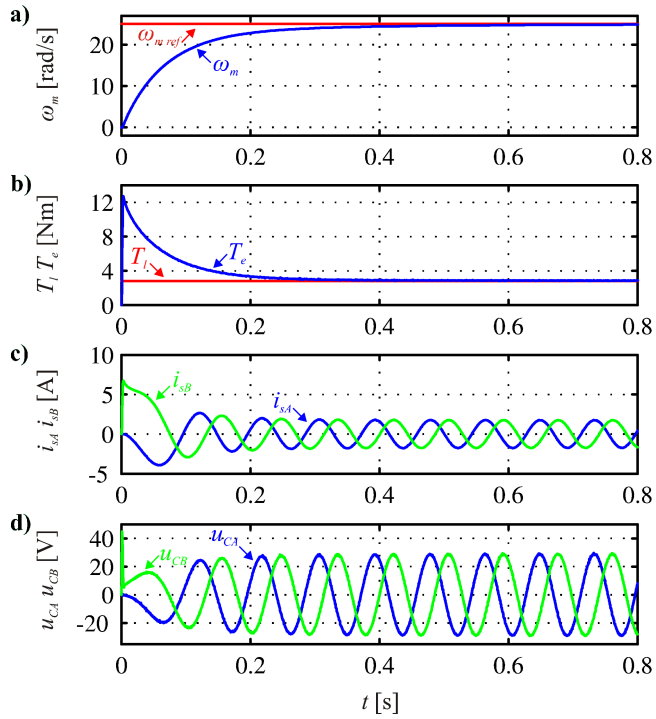

Fig. 7. Response of the PMSM drive with SFC1 to step change of the reference angular velocity

Step response of the PMSM drive fed from voltage control system with SFC1 is shown in Fig. 7a. Simulations were performed for constant load torque equal to 2.8 Nm. (Fig. 7b). As it can be seen, phase currents of the PMSM (Fig. 7c) as well as phase voltages (Fig. 7d) are sinusoidal in a steady-state. Phase currents of the PMSM don't exceed its nominal value during start-up.

3.2. State feedback control structure with internal model control, feedforward path and disturbance compensation (SFC2). Now a feedforward path from reference signals (i.e. $u_{Cd\,ref}$ and $u_{Cq\,ref}$) will be introduced to voltage control system in order to improve dynamic properties of the state feedback controller. Moreover, and additional feedback from measurable disturbance (i.e. i_{sd} and i_{sq}) will be also included. At first, residual model of state Eq. (8) should be introduced [13, 18]:

$$\frac{\mathrm{d}\widetilde{\boldsymbol{x}}}{\mathrm{d}t} = \boldsymbol{A}(\omega_k)\widetilde{\boldsymbol{x}} + \boldsymbol{B}\widetilde{\boldsymbol{u}}, \tag{18}$$

where

$$\widetilde{\boldsymbol{x}} = \boldsymbol{x} - \boldsymbol{x}_{ss}, \qquad \widetilde{\boldsymbol{u}} = \boldsymbol{u} - \boldsymbol{u}_{ss} \tag{19}$$

are deviations from the steady-state.

It should be noted, that residual model presented above is non-stationary due to the presence of angular velocity in the state matrix $\boldsymbol{A}$. Disturbance vector $\boldsymbol{d}$ is not present in residual model (18) because it was assumed that it remains constant for deviations from steady-state.

The control law for the residual model depicted above can be formulated as follows:

$$\boldsymbol{u} = -\boldsymbol{K}_x(\omega_k)\boldsymbol{x} + \begin{bmatrix} \boldsymbol{K}_x(\omega_k) & \boldsymbol{I} \end{bmatrix} \begin{bmatrix} \boldsymbol{x}_{ss} \\ \boldsymbol{u}_{ss} \end{bmatrix}, \tag{20}$$

where $\boldsymbol{I}$ denotes an identity matrix with an appropriate dimension. The column vector from the right-hand side of (20) can be calculated from the following form of the state equation rewritten in a steady-state:

$$\begin{bmatrix} \boldsymbol{x}_{ss} \\ \boldsymbol{u}_{ss} \end{bmatrix} = -\boldsymbol{G}(\omega_k)^{-1}\boldsymbol{H} \begin{bmatrix} \boldsymbol{d} \\ \boldsymbol{r} \end{bmatrix}, \tag{21}$$

where

$$\boldsymbol{G}(\omega_k) = \begin{bmatrix} \boldsymbol{A}(\omega_k) & \boldsymbol{B} \\ \boldsymbol{C} & \boldsymbol{0} \end{bmatrix}, \quad \boldsymbol{C} = \begin{bmatrix} \boldsymbol{0} & \boldsymbol{I} \end{bmatrix},$$
$$\boldsymbol{H} = \begin{bmatrix} \boldsymbol{E} & \boldsymbol{0} \\ \boldsymbol{0} & -\boldsymbol{I} \end{bmatrix}, \quad \boldsymbol{r} = \boldsymbol{r}_i.$$

After substituting of (21) into (20), the control law can be rearranged as follows:

$$\boldsymbol{u} = -\boldsymbol{K}_x(\omega_k)\boldsymbol{x} - \begin{bmatrix} \boldsymbol{K}_x(\omega_k) & \boldsymbol{I} \end{bmatrix} \boldsymbol{G}(\omega_k)^{-1}\boldsymbol{H} \begin{bmatrix} \boldsymbol{d} \\ \boldsymbol{r} \end{bmatrix}. \tag{22}$$

The control law with the feedforward path takes the following form:

$$\boldsymbol{u} = -\boldsymbol{K}_x(\omega_k)\boldsymbol{x} - \boldsymbol{K}_f(\omega_k) \begin{bmatrix} \boldsymbol{d} \\ \boldsymbol{r} \end{bmatrix}, \tag{23}$$

where $\boldsymbol{K}_f(\omega_k) = [\boldsymbol{K}_x(\omega_k)\boldsymbol{I}]\boldsymbol{G}(\omega_k)^{-1}\boldsymbol{H}$.

Finally, the discrete form of the control law with the non-stationary feedforward path and with an internal input model of the reference signals is given by:

$$u(n) = -\boldsymbol{K}_x(\omega_k)\boldsymbol{x}(n) - \boldsymbol{K}_{ec}(\omega_k)\boldsymbol{e}_c(n) - \boldsymbol{K}_f(\omega_k) \begin{bmatrix} \boldsymbol{d}(n) \\ \boldsymbol{r}(n) \end{bmatrix}. \tag{24}$$

If we assume that voltage control have to be realized in the linear range of modulation, gain matrices (15) cannot be directly used to calculate a state feedback controller with the feedforward path. The following values of penalty matrices (15) has been chosen to calculate SFC2 controller coefficients: $q_1 = q_2 = 1.6 \times 10^1$, $q_3 = q_5 = 1.3 \times 10^{-1}$, $q_4 = q_6 = 3 \times 10^{-1}$, $r_1 = r_2 = 6 \times 10^2$.

Just as for the SFC1 controller, it was assumed that SFC2 should provide: zero steady state error of u_{Cd} and u_{Cq} for step changes of u_{Cdref} and u_{Cqref}, achieve maximum permissible dynamics of voltage control in the linear range of modulation.

Non-stationary gain coefficients of the SFC2 were used to calculate feedforward gain values:

$$\boldsymbol{K}_f(\omega_k) = \begin{bmatrix} k_{f1}(\omega_k) & k_{f2}(\omega_k) & k_{f3}(\omega_k) & k_{f4}(\omega_k) \\ k_{f5}(\omega_k) & k_{f6}(\omega_k) & k_{f7}(\omega_k) & k_{f8}(\omega_k) \end{bmatrix}. \tag{25}$$

Coefficients: $k_{f1}(\omega_k)$, $k_{f3}(\omega_k)$, $k_{f6}(\omega_k)$, $k_{f8}(\omega_k)$ are quadratic functions of the angular velocity, $k_{f2}(\omega_k)$, $k_{f4}(\omega_k)$, $k_{f5}(\omega_k)$, $k_{f7}(\omega_k)$ are linear functions of the angular velocity respectively. Simulation tests were carried out in order to optimize coefficients of the SFC2 feedforward path. It was found, that the first and the sixth coefficient of (25) can be expressed as mean values of $k_{f1}(\omega_k)$ and $k_{f5}(\omega_k)$. Finally, values of (25) are as follows:

$$\begin{aligned} k_{f1} &= -0.1458, \\ k_{f2}(\omega_k) &= 2.8241 \times 10^{-5}\omega_k, \\ k_{f3}(\omega_k) &= 1.6404 \times 10^{-9}\omega_k^2 - 0.0175, \\ k_{f4}(\omega_k) &= 8.4211 \times 10^{-6}\omega_k, \\ k_{f5}(\omega_k) &= -2.8241 \times 10^{-5}\omega_k, \\ k_{f6} &= -0.1458, \\ k_{f7}(\omega_k) &= -8.4211 \times 10^{-6}\omega_k, \\ k_{f8}(\omega_k) &= 1.6404 \times 10^{-9}\omega_k^2 - 0.0175. \end{aligned} \tag{26}$$

Similar to SFC1 design procedure depicted below, all values of SFC2 controller's matrices $\boldsymbol{K}_x(\omega_k)$ and $\boldsymbol{K}_{ec}(\omega_k)$ were expressed as mean values of non-stationary coefficients:

$$\boldsymbol{K}_x = \begin{bmatrix} 0.14 & 0 & 0.0008 & 0 \\ 0 & 0.14 & 0 & 0.008 \end{bmatrix},$$
$$\boldsymbol{K}_{ec} = \begin{bmatrix} 0.017 & 0 \\ 0 & 0.017 \end{bmatrix}. \tag{27}$$

Block diagram of the described above state feedback controller with feedforward path (SFC2) was shown in Fig. 8.

Similar to SFC1 simulation tests, at the beginning the accuracy of the voltage shaping have been investigated. Results for SFC2 are shown in Fig. 9.

Proper operation of the designed voltage control system with SFC2 has been presented in Fig. 9b. The 5% settling time of u_{Cq} is about 1.1 ms. Similarly to control system with SFC1, dynamic properties of the presented voltage control loop are limited by the maximum permissible value of the control signal (i.e. $|u_{pd}| \leq 1$ and $|u_{pq}| \leq 1$). Due to the presence of the feedforward path in SFC2 controller, control signal u_{pq} (Fig. 9d) changes more rapidly in comparison to u_{pq} calculated by SFC1 (Fig. 6d). It should be noted that phase voltages presented in Fig. 9c are sinusoidal in a steady-state.

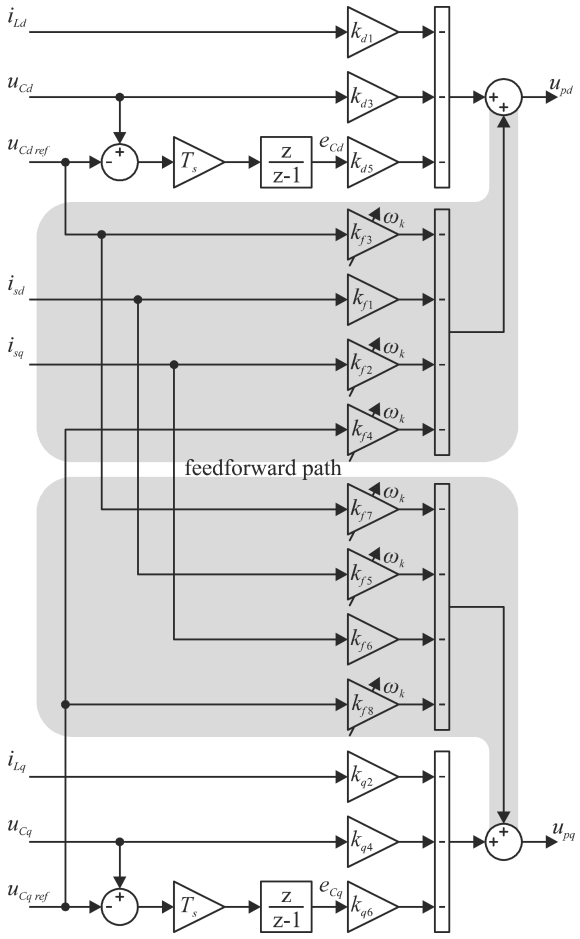

Fig. 8. Block diagram of the designed state feedback controller (SFC2)

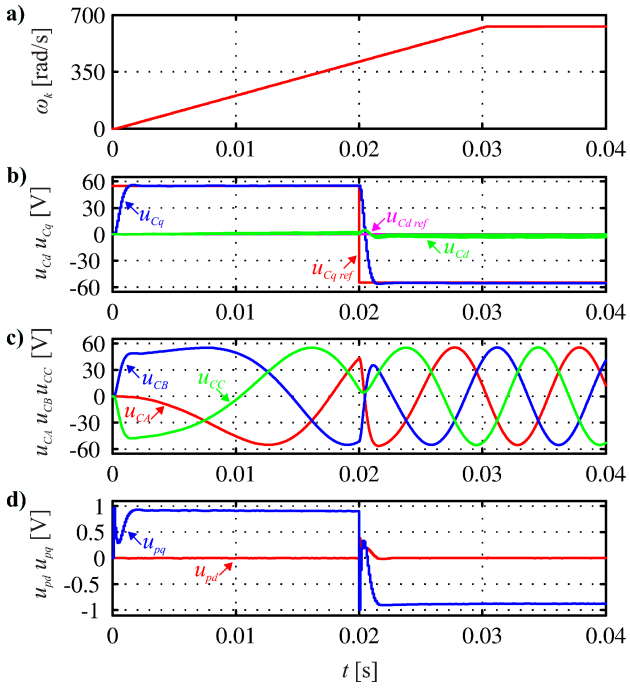

Fig. 9. Response of voltage control loop with SFC2 to step change of reference voltage $u_{Cq\,ref}$ and linear change of angular velocity ω_k

The operation of PMSM drive fed from a voltage control system (Fig. 3) with SFC2 has been illustrated in Fig. 10.

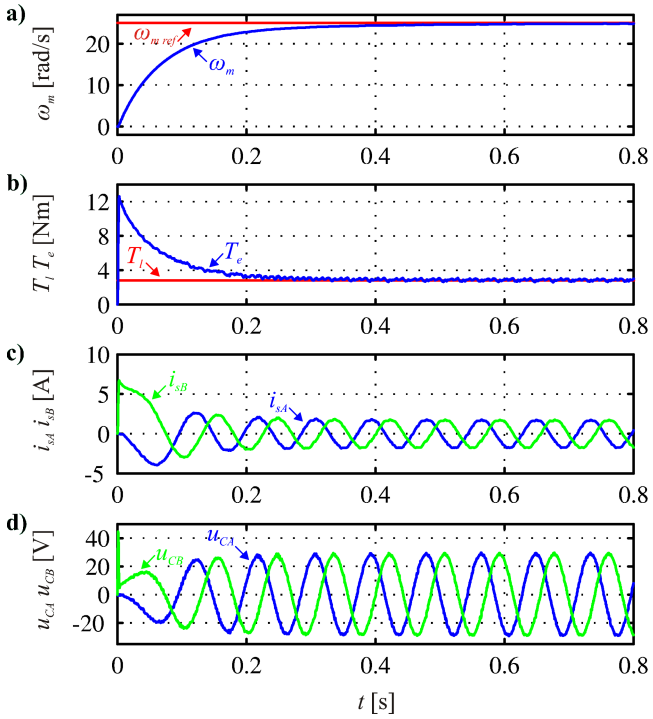

Fig. 10. Response of the PMSM drive with SFC2 to step change of the reference angular velocity

Step response of the PMSM drive fed from voltage control system with SFC2 is shown in Fig. 10a. The simulation conditions (step change of the angular velocity from 0 to 25 rad/s at 0 s and constant value of load torque) were the same as for the PMSM drive with SFC1 test (Fig. 7). It should be mentioned that, phase currents of the PMSM (Fig. 10c) as well as phase voltages (Fig. 10d) are sinusoidal during steady-state operation of the PMSM.

3.3. Torque ripple analysis Designed state feedback controllers SFC1 and SFC2 were examined in terms of PMSM torque ripple minimization.

In order to evaluate the effectiveness of the proposed state feedback control structures for torque ripple minimization, the torque ripple factor (*TRF*) defined as the ratio of the peak-to-peak torque ripple to the rated torque of the PMSM was introduced [2].

Figure 11a shows enlarged parts of the PMSM electromagnetic torque waveform observed for control systems with SFC1 and SFC2 in a steady-state respectively.

It can be seen that for SFC2 the torque consists of significant ripple and the corresponding *TRF* is approximately 2.114%. When SFC1 controller is used in a voltage control system, torque ripple is smaller and *TRF* = 0.864%. It will result in reduced motor mechanical vibration and acoustic noise [19].

Finally, steady-state PMSM torque spectrum for voltage control system with SFC1 and SFC2 is shown in Fig. 11b. We can see that harmonics are reduced after applying the SFC1 control scheme. Better torque ripple reduction observed for control system with SFC1 is mainly related to higher values of the gain matrix $\boldsymbol{K}_{ec}$ (17) with comparison to $\boldsymbol{K}_{ec}$ of SFC2 (27).

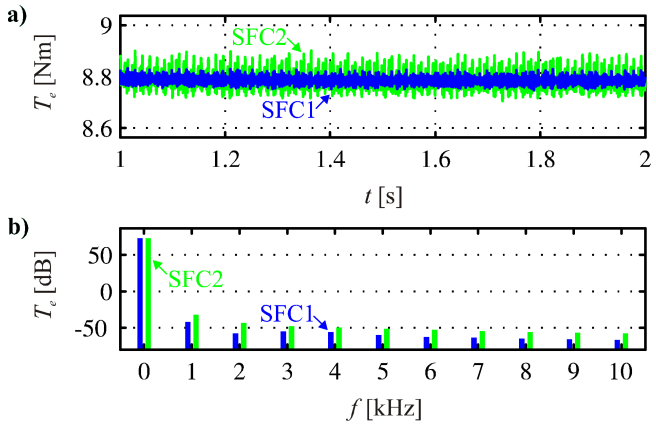

Fig. 11. Simulated steady-state PMSM torque waveform (a) and spectrum (b) at $\omega_m = 25$ rad/s with $T_{eN} = 8.8$ Nm

4. Experimental results

The designed state feedback voltage control system with SFC1 has been investigated experimentally in the laboratory drive system that consist of 2.76 kW PMSM supplied by the 3-level NPC type voltage source inverter with an output LC filter. The proposed SFC1 scheme as well as FOC scheme were implemented in a TMS320F28335 DSP. Control signals for IGBTs are generated with the help of XC6SLX9 FPGA. The conditioning interface of designed drive system includes: conditioning current and voltage signals from sensors to voltage in appropriate range for DSP, encoder interface (Hyperface). Communication between DSP and FPGA is realized by using the parallel bus. Block scheme of laboratory setup is presented in Fig. 12.

Experimental results for a voltage control system with the SFC1 control algorithm are shown in Fig. 13. It should be noted that the results of experiments are similar to simulation test results presented in Fig. 6.

Shown in Fig. 13b space vector components of the filter output voltages are controlled properly. Observed in Fig. 13b the 5% settling time of u_{Cq} is about 2.3 ms due to 10% overshoot. It should be noted that phase voltages presented in Fig. 13c are sinusoidal during steady-state operation of inverter. Shown in Fig. 13d control signals do not exceed the maximum permissible value.

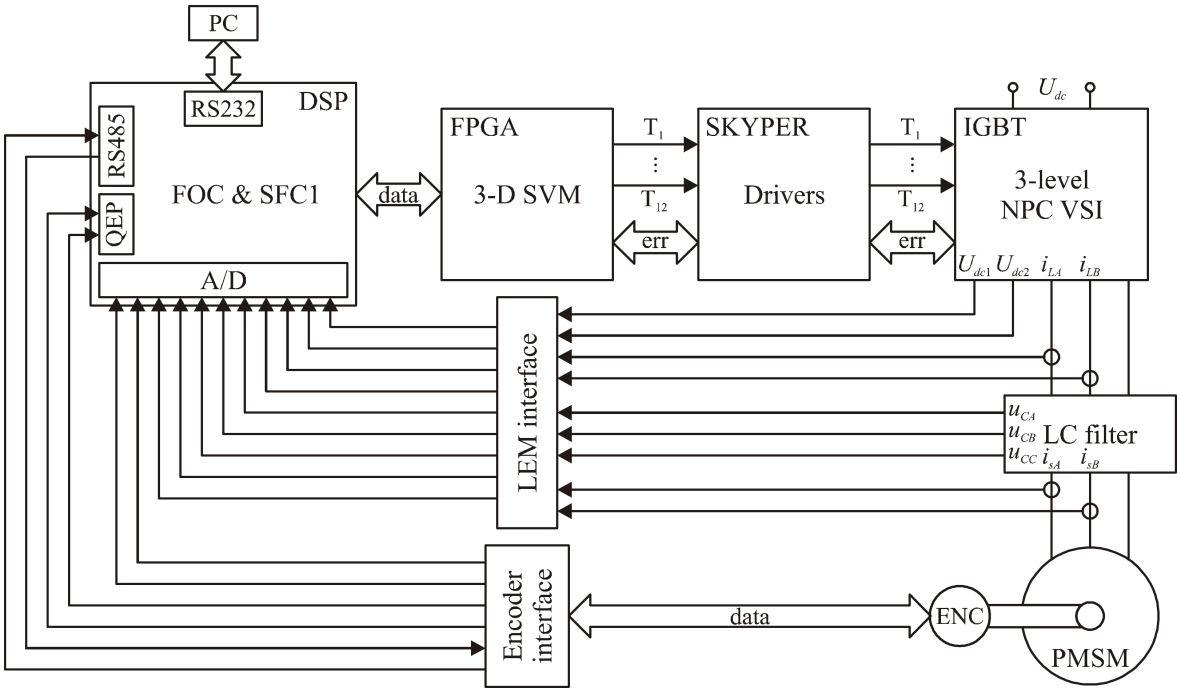

Fig. 12. Block scheme of laboratory setup

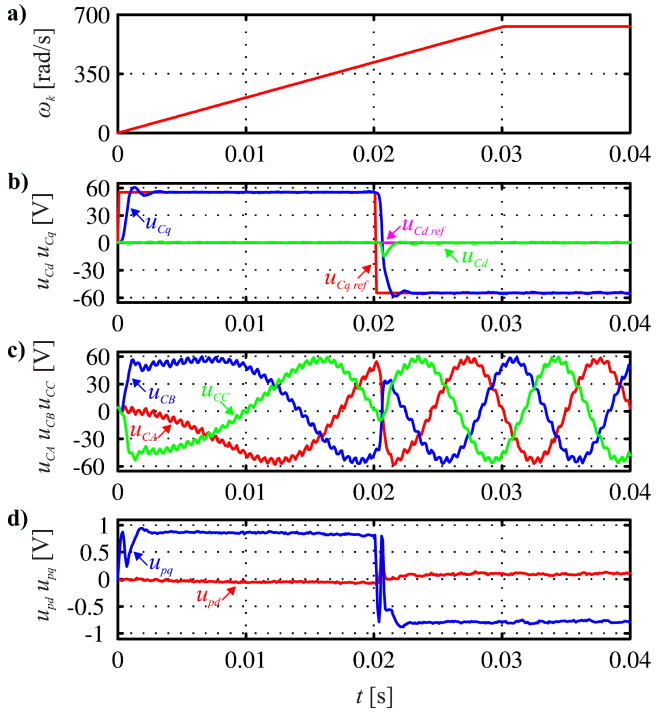

Fig. 13. Response of voltage control loop with SFC1 to step change of reference voltage $u_{Cq\,ref}$ and linear change of angular velocity ω_k

Finally, the proper operation of PMSM drive fed from voltage control system with SFC1 has been shown in Fig. 14.

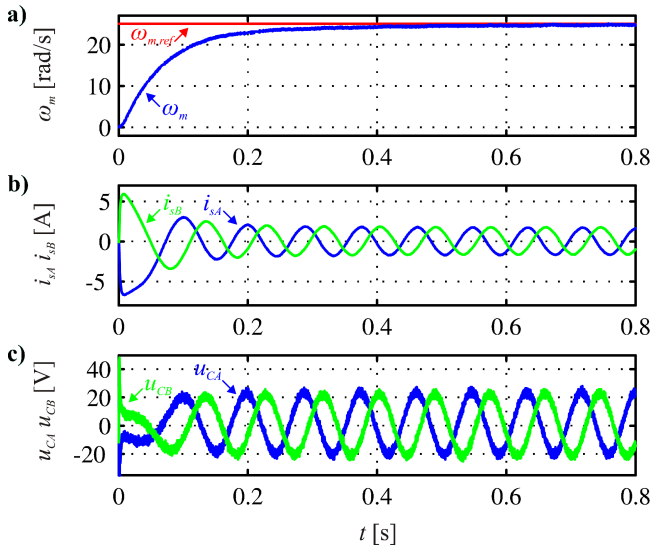

Fig. 14. Response of the PMSM drive with SFC1 to step change of the reference angular velocity

5. Conclusions

It was found that a non-stationary state feedback controller in a voltage control system that provides a continuous voltage shape waveform can be replaced by the stationary one without deteriorate voltage control performance.

When a linear range of the modulator operation is taken into account during a synthesis procedure of the state feedback controller, better reduction of a torque ripple can be achieved for the SFC1 control structure. It was found that an integral action of the state feedback controller has to be limited when a feedforward path is applied. Only in this case SFC2 produces control signals in a linear range of modulator. Weak integral action of the SFC2 causes worse torque ripple reduction in comparison to SFC1. Moreover, a feedforward path of the SFC2 should be non-stationary (it depends on ω_k) in order to obtain proper voltage control.

Dynamic properties of a voltage control system are almost the same when SFC1 as well as SFC2 is used.

Obtained simulation and experimental results indicate that the designed state feedback voltage controller properly shapes continuous voltage of the NPC type 3-level inverter.

Acknowledgements. Research work financed by the National Science Centre (Poland) under the Grant no. 6636/B/T02/2011/40 (from 2011 to 2013).

REFERENCES

[1] T.M. Jahns and W.L. Soong, "Pulsating torque minimization techniques for permanent magnet AC motor drives-a review", *IEEE Trans. on Ind. Electronics* 43 (2), 321–330 (1996).

[2] W. Qian, S.K. Panda, and J.X. Xu, "Torque ripple minimization in PM synchronous motors using iterative learning control", *IEEE Trans. on Power Electronics* 19 (2), 272–279 (2004).

[3] S.K. Panda, J.X. Xu, and W. Qian, "Review of torque ripple minimization in PM synchronous motor drives", *Proc. Power and Energy Society General Meeting-Conversion and Delivery of Electrical Energy in the 21st Century* 1, 1–6 (2008).

[4] V. Petrovic, R. Ortega, A.M. Stankovic, and G. Tadmor, "Design and implementation of an adaptive controller for torque ripple minimization in PM synchronous motors", *IEEE Trans. on Power Electronics* 15 (5), 871–880 (2000).

[5] J.Y. Hung and Z. Ding, "Design of currents to reduce torque ripple in brushless permanent magnet motors", *IEE Proceedings-B Electric Power Applications* 140 (4), 260–266 (1993).

[6] M. Kojima, K. Hirabayashi, Y. Kawabata, E.C. Ejiogu, and T. Kawabata, "Novel vector control system using deadbeat-controlled PWM inverter with output LC filter", *IEEE Trans. on Industry Applications* 40 (1), 162–169 (2004).

[7] J.K. Steinke, "Use of an LC filter to achieve a motor-friendly performance of the PWM voltage source inverter", *IEEE Trans. on Energy Conversion* 14 (3), 649–654 (1999).

[8] N. Celanovic and D. Boroyevich, "A comprehensive study of neutral-point voltage balancing problem in three-level neutral-point-clamped voltage source PWM inverters", *IEEE Trans. on Power Electronics* 15 (2), 242–249 (2000).

[9] K. Kulikowski and A. Sikorski, "Efficiency improvement due to direct torque and flux three levels three areas control method applied to small hydroelectric power plant", *Bull. Pol. Ac.: Tech.* 59 (4), 569–574 (2012).

[10] A. Sikorski, K. Kulikowski, and M. Korzeniewski, "Modern Direct Torque and Flux Control methods of an induction machine supplied by three-level inverter", *Bull. Pol. Ac.: Tech.* 61 (4), 771–778 (2013).

[11] J. Salomaki, M. Hinkkanen, and J. Luomi, "Sensorless control of induction motor drives equipped with inverter output filter", *IEEE Trans. on Ind. Electronics* 53 (4), 1188–1197 (2006).
[12] T. Tarczewski and L.M. Grzesiak, "PMSM fed by 3-level NPC sinusoidal inverter with discrete state feedback controller", *Proc. 15th Eur. Conf. on Power Electronics and Applications, EPE 2013* 1, 1–9 (2013).
[13] A. Pawlikowski and L. Grzesiak, "Vector-controlled three-phase voltage source inverter producing a sinusoidal voltage for AC motor drives", *Proc. The Int. Conf. on "Computer as a Tool" EUROCON 2007* 1, 1902–1909 (2007).
[14] L.M. Grzesiak and T. Tarczewski, "PMSM servo-drive control system with a state feedback and a load torque feedforward compensation", *COMPEL* 32 (1), 364–382 (2013).
[15] R. Krishnan, *Permanent Magnet Synchronous and Brushless DC Motor Drives*, CRC Press, London, 2010.
[16] L.M. Grzesiak and T. Tarczewski, "Permanent magnet synchronous motor discrete linear quadratic speed controller", *Proc. IEEE International Symposium on Industrial Electronics, ISIE 2011* 1, 667–672 (2011).
[17] A. Tewari, *Modern Control Design with MATLAB and SIMULINK*, Wiley, Chichester, 2002.
[18] D.C. Lee, S.K. Sul, and M.H. Park, "High performance current regulator for a field-oriented controlled induction motor drive", *IEEE Trans. on Industry Applications* 30 (5), 1247–1257 (1994).
[19] K. Gulez, A.A. Adam, and H. Pastaci, "Torque ripple and EMI noise minimization in PMSM using active filter topology and field-oriented control", *IEEE Trans. on Industrial Electronics* 55 (1), 251–257 (2008).